J Porous Mater (2017) 24:109–120
DOI 10.1007/s10934-016-0243-7

Zirconium incorporated micro/mesoporous silica solid acid catalysts for alkylation of *o*-xylene with styrene

Mingyu Zhang[1] · Xiaoli Sheng[1] · Yiwei Zhang[1] · Yuming Zhou[1] · Shuo Zhao[1] · Xiaoqin Fu[1] · Hongxing Zhang[1]

Published online: 15 July 2016

Abstract The design of micro/mesoporous silica materials with solid acid catalysts for the catalytic reactions can inject new vitality into the development of nanostructures. In this paper, zirconium was successfully incorporated into micro/mesoporous silica by the direct hydrothermal synthesis, employing P123 and protic ionic liquid as the structure-directing agent. The physico-chemical properties of the micro/mesoporous silica-zirconia were characterized by means of X-ray scattering, N_2 gas sorption, scanning electron microscopy, transmission electron microscopy and NH_3 desorbed TPD methods. The influence of Si/Zr ratio and different calcination temperature on the acidity and catalytic properties were discussed. Also, the catalytic activities of solid acid catalysts were evaluated by the alkylation of *o*-xylene with styrene. The results indicate that the heteroatom of zirconium has been successfully incorporated into the structure framework and the solid acid catalysts still possess hierarchically porous structure. The prepared catalytic materials contain moderate to strong acid sites, meanwhile, the amount of strong acid sites increases with a decrease of Si/Zr ratio. The SZ-10-SO_4^{2-} (molar ratio of Si/Zr = 10) catalyst was found to be the most promising and gave the highest selectivity among all catalysts, which was due to the strong interaction between H_2SO_4 and micro/mesoporous materials in the presence of Zr, thus prevent H_2SO_4 leaching from the materials. It is worth noting that SZ-10-937 (calcined at 937 K) also has the higher yield of PXE, which maybe the enhancement of crystallization of tetragonal ZrO_2 made the strong acid sites for SZ-973 sample be more than that of the other samples with the increase of calcination temperature.

Keywords Micro/mesoporous materials · Silica-zirconia · Protic ionic liquid · Alkylation reaction · Solid acid catalyst

1 Introduction

Acid catalysts play an important role in organic synthesis. Many organic reactions such as alkylation, isomerization, esterification, cracking, etc. are accomplished by acid catalysts. Conventionally, these reactions were carried out by homogeneous catalysts, for instance, H_2SO_4, BF_3, HF or $AlCl_3$, however, the use of liquid acid catalysts encountered some disadvantages like increasing waste disposal costs, heavy environmental pollution, corrosiveness and low reaction selectivity [1–3]. Many efforts have been made to exploit the environmentally friendly catalytic technology for the reaction. Recently, using heterogeneous catalysts in liquid phase reaction has received great attention owing to some advantages of solid acid catalysts for such as high reactivity, environmental friendliness and easy to recover and reuse [4–6], and numerous efforts have been made with novel heterogeneous solid acid catalysts to replace traditional liquid catalysts.

Alkylation of *o*-xylene with styrene has received great interest due to the immense application of the 1-phenyl-

Electronic supplementary material The online version of this article (doi:10.1007/s10934-016-0243-7) contains supplementary material, which is available to authorized users.

✉ Yiwei Zhang
zhangchem@seu.edu.cn

✉ Yuming Zhou
ymzhou@seu.edu.cn

[1] School of Chemistry and Chemical Engineering, Southeast University, Jiangsu Optoelectronic Functional Materials and Engineering Laboratory, Nanjing 211189, People's Republic of China

larylethane (PXE). PXE is widely used as a high-energy fuel for turbojets, jets, rockets, missile engines, as a high-stability lubricant and as an important additive in the corrosion protective coatings of chlorinated rubber and synthetic resins [1]. For PXE synthesis, solid acids such as silica-alumina [4], ion-exchange resins [5] and sulfated zirconia/titania [6] have been used as catalysts. Among these solid acid catalysts, they exhibit good performance, but they are unstable at high reaction temperature. Microporous materials have high thermal stability and high acidity, however, the microporous materials possess small pore size, which limits their wide applications.

Hierarchical porous materials have received significant attention due to their important roles in the systematic study of structure property relationship and their technological promise in applications [7, 8]. They exhibit at least two types of pores, and the designed micro/mesoporous materials can further improve their structure order as well as the thermal, hydrothermal and mechanical stability [9]. Since mesoporous silica materials were discovered [10], the properties of mesoporous silica materials have been extensively studied by many authors due to their wide range of applications [11, 12]. Furthermore, the metal incorporated/functionalized catalysts obtained by mesoporous silica material as support have been reported, which incorporated catalytic species such as V [13], Cu [14], Ti [15] and Zr [16]. The incorporation of mental ions, in general, creates acid sites in mesoporous materials. For instance, Maheswari et al. [16] obtained a series of mesostructured Zr-SBA-16 with different Si/Zr ratio by using Pluronic F127 triblock copolymer as a structure directing agent. They successfully incorporated Zr^{4+} ions without any pH adjustments up to 6.5 wt% of Zr loading. The acidity of SBA-16 is only 0.02 NH_3/g [17]. While with an increasing Zr loading, ammonia desorption rise and thus the total acidity of Zr-SBA-16 samples increases to 0.21–0.55 mmol NH_3/g. Moreover the activity of Zr-SBA-16 is probed as catalysts in a one-pot synthesis reaction. The results demonstrate that those catalysts exhibit the high catalytic activity and successive recycle runs. So far, with development of a variety of binary metallic based on mesoporous silica materials, Zr doping is one of the most promising ways because of their fascinating characteristics and many applications, which include alkali-durable glasses [18], catalyst support [19, 20] and advanced ceramic material [21]. The introduction of Zr not only maintains their original structural characteristics but also endows the resultant material with additional properties [22, 23]. Notably, ZrO_2 is an amphoteric oxide with a monoclinic structure at room temperature [23], which changes reversibly to tetragonal [24] and then cubic (distorted fluorite) modifications at higher temperatures. Therefore, an appropriate synthesis method is necessary to obtain the desired materials. During the past decades, tremendous efforts have been devoted to design micro/mesoporous materials by using different approaches [22–26]. The approach using templates has been considered as one of the most promising methods to prepare this kind of hierarchical porous materials [27].

Recently, ionic liquids (ILs) which are molten salt at room temperature have received considerable attention in many areas of chemistry and industry due to their superior properties such as high thermal stability, non-flammability, and negligible vapor pressure, etc. [26–30]. ILs can play some roles in chemistry, organometallic, biocatalyzed reaction and other fields [31]. It is reported that ILs are able to act as multiple pores of cosolvent, cosurfactant as well as salt in the system [31–33]. More importantly, ILs can act as template to induce micropores or mesopores. In the previous work, these materials were mostly prepared by imidazolium based ILs. Hu et al. [9] utilized CTAB and IL-C4 ($[C_n mim]Br$) mixtures as the dual templates to synthesize a series of micro/mesoporous materials. They elucidate the formation mechanism by studying the interaction between CTAB and IL-C4 based on the measurement of the cmc of the CTAB/$[C_4 mim]Br$ mixture aqueous solutions at different compositions and temperatures. Highly ordered mesoporous silica and Ru/SiO_2 with high surface area have been synthesized by Zhu et al. [34] via 1-hexadecyl-3-methyl-imidazolium chloride as template under strong acidic and basic conditions. Hence, imidazolium based ILs can induce micro or mesoporous materials [35–37]. However, there are few reports on the synthesis of micro/mesoporous materials by using protic ionic liquids (PIL) which are formed via the proton transfer from a Bronsted acid to a Bronsted base. Zhao et al. [32] synthesized the micro/mesoporous silicate materials using P123 and PILs (triethylamine acetate) as the co-template. They find when the content of PIL is low, P123 and PIL are miscible and can form mixed micelles in aqueous. When the content of PIL is increased, the PIL can be separated from the mixed micelles and self-assembled to the new micelles which acted as microporous templates.

In the present work, we report that zirconium element has been successfully incorporated into silicate framework. The micro/mesoprous materials were prepared with P123 and PIL (n-tributylamineacetate) as the co-template. Meanwhile, several solid acid catalysts were prepared by the impregnation method and their catalytic activities were evaluated by the alkylation of *o*-xylene with styrene. A series of samples were synthesized by changing Si/Zr ratios and the calcination temperature. The aim of this paper is to show the effect of zirconium-doped silica on the performance of catalysts.

2 Experimental section

2.1 Chemicals

(Ethylene oxide) triblock copolymer Pluronic P123 ($EO_{20}PO_{70}EO_{20}$, Mw = 5800) was purchased from Sigma-Aldrich, The inorganic precursor was silicon (IV) tetraacetate (TEOS 97 %, Fluka), inorganic Zr-containing salt ($Zr(NO_3)_4{\cdot}5H_2O$, Aldrich) and HCl (37 % in water, Aldrich) was used as the reaction catalyst, n-tributylamine (Merck) and acetic acid (Merck) were used to synthesis PIL. Water used in the synthesis was distilled and deionized.

2.2 Preparation of PIL

N-tributylamine acetate was obtained by an acid–base neutralization method. The typical synthesis process is described as following: acetic acid (30.025 g) was added into n-tributylamine (92.675 g) dropwise under vigorous stirring at 333 K for 8 h. The obtained yellow liquid was characterized by 1H NMR ($CDCl_3$) δ:7.259 (s 1H, –NH), 1.969 (s, 3H, CH_3COO^-), 2.84 (s, 2H, N–CH_2–), 1.589 (m, 2H, –C–CH_2–C–), 1.286 (m, 2H, –CH_2–C), 0.922 (t, 3H, –CH_3).

2.3 Synthesis of micro/mesoporous materials

The materials were synthesized by a hydrothermal method. And TEOS plays as silica source, $Zr(NO_3){\cdot}5H_2O$ as zirconium source, P123 and PIL are structure-directing agent. A typical synthesis was: 4 g P123 and 2.67 g PIL (PIL/(PIL + P123) = 40, detailed in Fig. S1) were completely dissolved in 80 ml deionized water, whose pH was controlled by HCl (2 M). Under vigorous stirring, appropriate amount of $Zr(NO_3)_4{\cdot}5H_2O$ were slowly added with stiring. Then 9 gtetraethyl orthosilicate (TEOS) was dripped slowly. After stirring at 313 K for 24 h, a gel was obtained. Then the whole slurry was transferred to a 100 ml Teflon-lined stainless steel autoclave for aging at 393 K for 48 h. The product was recovered by filtration washed with ethanol and deionized water, and dried in an oven overnight. Finally, the white as-synthesized solid powders were calcined at appropriate temperature for 6 h in ambient air to remove the template. The pure micro/mesoporous silica material was prepared using the same method without the addition of $Zr(NO_3)_4{\cdot}5H_2O$.

Similarly, a series of micro/mesoporous materials were synthesized by changing the the Si:Zr molar ratio and calcination temperature during synthesis. The final products were denoted as SZ–*X*–*Y*, where *X* stands for the molar ratio of Si to Zr and *Y* represents the calcination temperature. The sulfated samples were denoted as SZ–*X*–*Y*-SO_4^{2-}.

2.4 Preparation of solid acid catalysts

Solid acid catalysts were prepared by the wet impregnation method. Typically, 2 g uncalcined solid product was further immersed into 1 M H_2SO_4 solution at room temperature for 6 h, followed by drying at 373 K overnight and calcining at 823 K for 6 h in air.

2.5 Catalytic tests

The catalytic activity of each sample was evaluated in terms of the alkylation reactions, which was carried out in a continuously stirred oil batch reactor under 393 K. The quality ratio of styrene to *o*-xylene was 7.5:1, and the amount of catalyst was 2 % of the total mass. At first, a small fraction of *o*-xylene, and the suitable amount of catalyst were introduced in a three-neck 100 mL round-bottom flask equipped with a condenser and magnetic stir bar, then the mixture of a certain amount of styrene and the remained *o*-xylene was added dropwised into the flask for 2 h. Finally, the mixture maintained for another 1 h. After the reaction was completed, the mixture cooled down to room temperature, filtered to separate the catalysts. The crude product was distilled under atmospheric pressure to remove the remaining *o*-xylene. Then the liquid was analyzed with GC-9890A gas chromatograph equipped with OV-1 capillary column and a flame ionization detector (FID). The yield of PXE was defined as follows:

$$\text{Yield of PXE}\,(\%) = \text{actual product weight}/\text{theoretical product weight} \times 100\,\%$$

$$\text{Actual product weight} = \text{crude product weight} \times \text{PXE(chromatography)}\%$$

2.6 Characterization

The crystal phase of micro/mesoporous SiO_2–ZrO_2 was characterized by an X-ray diffractometer (Rigaku, RINT-Ultima III) using Cu Kα radiation with 40 kV and 200 mA. All scans were continuous and ran between 2θ values of 0.5°–5° and 10°–80°. Transmission electron microscopy (TEM) images were obtained using FEI Tecnai G20 instrument. N_2 adsorption–desorption isotherms were obtained at 77 K with ASAP 2020 apparatus (Micromeritics USA) by means of the Brunauer–Emmett–Teller (BET) method. Micropore volume was calculated by the t-plot method. The pore size distribution in mesopore range was analysed by the BJH (Barrett–Joyner–Halenda) method using the Halsey equation for multilayer thickness.

Micropore volume was calculated by the t-plot method. NH_3 temperature-programmed desorption (NH_3-TPD) profiles of the samples were carried out on a TP-5000 adsorption instrument made in china.

3 Results and discussion

3.1 Effect of the Si/Zr

A contrast among the low-angle XRD patterns of the samples induced by PIL/P123 co-template with different Si/Zr is presented in Fig. 1. The samples SZ-20, SZ-40 and SZ-10 display three reflections, a strong reflection and two other weaker reflections, which corresponds to the (100), (110) and (200) reflections, respectively. Furthermore, the intensities of characteristic peaks weaken with the increase of Zr content in the samples, suggesting that the porous ordering decreased gradually with the increasing of Zr content. The reason for this phenomenon may be the partial collapse of the cubic ordered phase aroused by the incorporation content increasing of Zr species. The sample SZ-5 only possesses one diffraction peak and SZ-3 has no obvious diffraction peak, which suggests the order structure has been destroyed. That is to say, the content of zirconium can affect the sample's structure.

Figure 2a shows the high angle X-ray powder diffraction patterns of the samples calcined at 823 K with different Si/Zr. The XRD patterns demonstrate that the materials are amorphous. No significant shifts of the principal diffraction peaks are observed except for the characteristic silica hump, proof for successful incorporation of Zr atoms. Thus, no significant diffraction peaks indicative

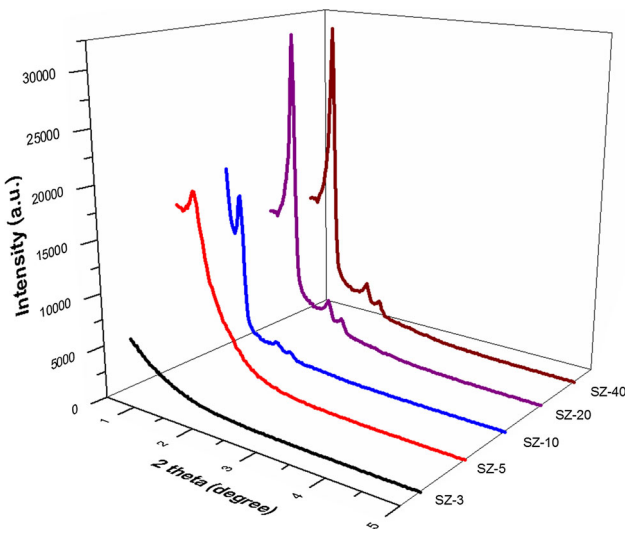

Fig. 1 Small-angle XRD pattern of the samples with different Si/Zr calcined at 823 K

of Zr can be observed even for SZ-10 sample. Samples SZ-5 and SZ-3 display three sharp peaks which verify the extensive crystallization of ZrO_2. Further, the intensities of the characteristic peaks weaken with the decrease of Zr content in the samples, indicating that the diffraction peak intensity varies with the increasing of ZrO_2 crystallized. Meanwhile, the chemical composition of the sample SZ-10 was investigated by EDX spectroscopy analysis (Fig. S2). Moreover, it is also noticed that the samples immersed in H_2SO_4 solution have no ZrO_2 diffraction peak, implying that the ZrO_2 reacted with H_2SO_4 and the Zr^{4+} and SO_4^{2-} exist in the micro/mesoporous structure. The hump observed between $2\theta = 15°–30°$ is due to amorphous nature of silica network.

N_2 adsorption–desorption isotherms of the samples for various samples are shown in Fig. 3. All of the isotherms exhibit the typical IV adsorption with N_2 hysteresis characteristic of mesoporous materials with large uniform cage-type porosity, according to the IUPAC classification [16], illustrating that the synthesized samples have a ordered porous structure. The shape of the isotherms varies with the different Si/Zr ratios. With the increase of Zr, the starting point of the hysteresis gradually reduces, which suggests the structure of order channel is less ordered and formed some narrower pores. It can be seen that the sample SZ-3 possesses a distorted hysteresis loop which demonstrates the loss of order pore structure. The sulfated samples still have type H1 hysteresis loop, illustrating the samples keep a well-organized mesoporous structure, as shown in Fig. 3b. But the starting point of the hysteresis has reduced, indicating that the less ordered structure compared with the samples without H_2SO_4 acidification.

Figure 4a shows the pore size distribution calculated by BJH model which is based on desorption curves. From the data, it can be observed that narrow pore size distribution and that pore volume decreases with the increase of the Zr content. The phenomenon illustrates that zirconium occupies parts of the channel structure which disperses relatively evenly, thus corresponding pore volume reduces. It is worth noticing that two peaks were observed from the pore size distributions of the sample SZ-10, whereas the others have only one peak. The difference may be caused by the existence of PIL and P123 which act as micropore template and mesoporous template, respectively. Though all the materials obtained with the same content of PIL and P123, they have different zirconium content. With the excessive amount of zirconium, ZrO_2 occupies parts of the channel structure so that the pore size becomes smaller. With the less zirconium content, only some smaller pores are occupied, so the materials showed a multitude of mesopores. When the amount of zirconium is suitable, the pores with different size are exposed. As shown in Fig. 4b, the pore sizes of the sulfonated samples decrease compared

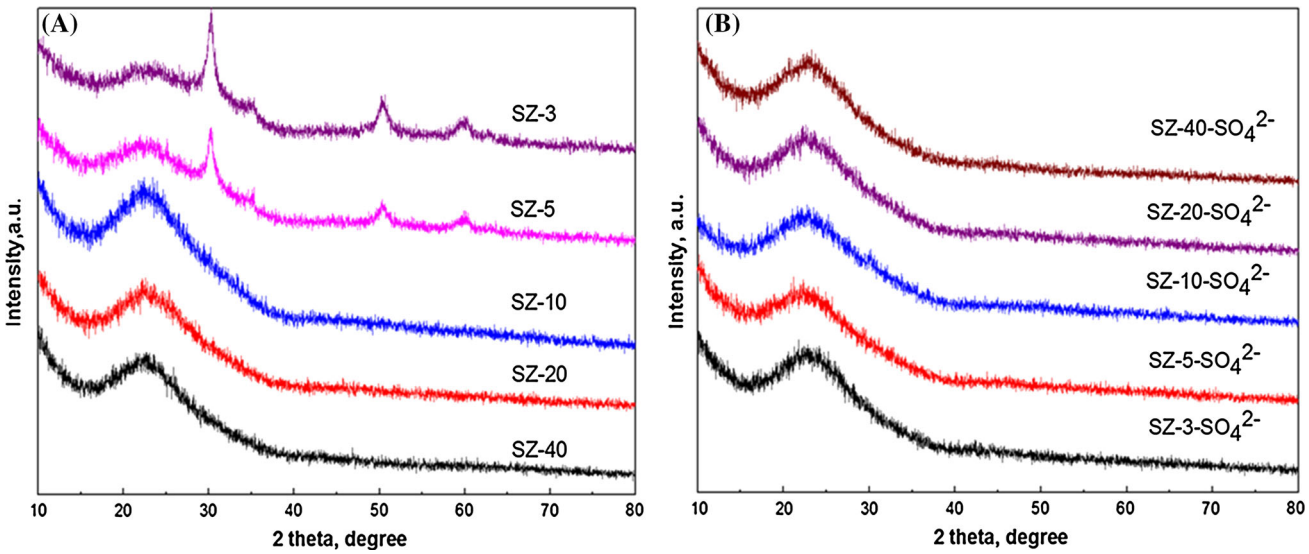

Fig. 2 XRD pattern of the samples with different Si/Zr calcined at 823 K. **a** Without H_2SO_4 acidification. **b** After H_2SO_4 acidification

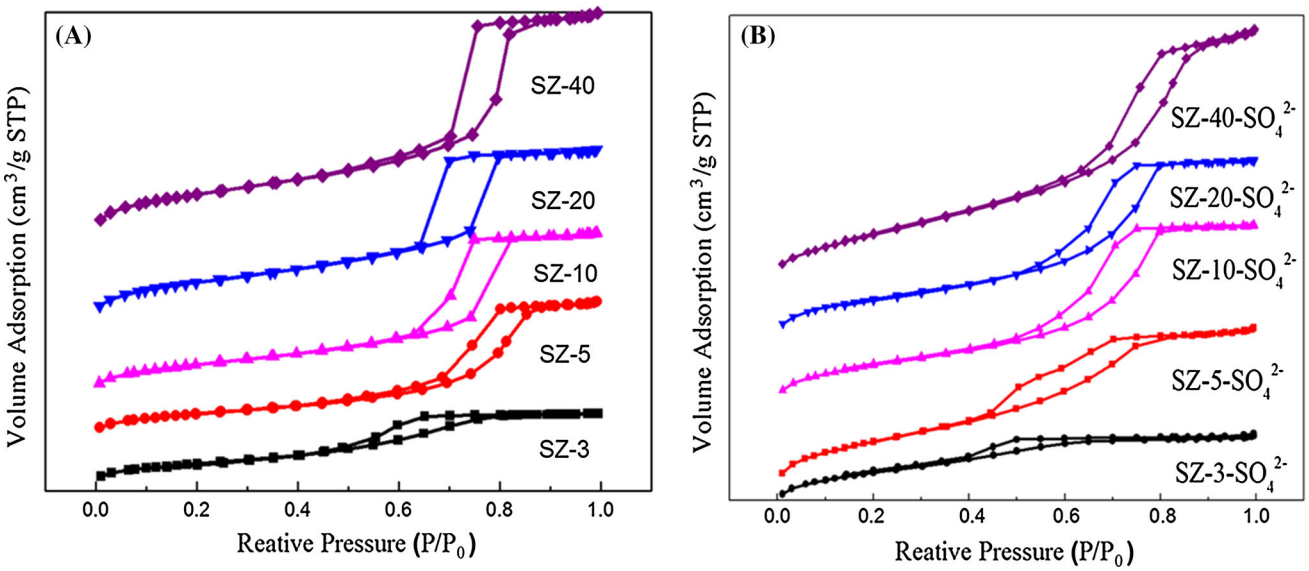

Fig. 3 N_2 adsorption–desorption isotherms with different Si/Zr calcined at 823 K. **a** Without sulfonated. **b** After the sulfonated

with SZ-3 and SZ-5, suggesting that more narrower pores appeared after sulfonated.

The characteristic data of the surface area, the microporous surface area, the BJH cumulative pore volume and the average pore diameter are summarized in Table 1. The BET surface area and average pore sizes of materials without sulfonation decreases with increasing zirconia content: the surface areas decrease from 829 to 412 m^2/g and the average pore sizes decrease from 7.35 to 4.48 nm. The dramatic decrease in surface areas with increasing of Zr loading indicates that pore blocking may be occurring as ZrO_2 nanoparticles are deposited into the pores of the materials. In addition, the very high Zr loadings (SZ-3) in materials may have resulted in a collapse of the pore structure thus giving rise to the observed decrease in the surface areas. Through the analysis, it is known that the well-organized mesochannel can be obtained with appropriate Zr content. However, SZ-3-SO_4^{2-} and SZ-5-SO_4^{2-} show higher specific surface, pore areas and average pore diameter decrease and also indicates the samples with lower Zr content have less effect on H_2SO_4. The reason for this phenomenon may be that most of the covered narrower pores exposed after ZrO_2 nanoparticles which are deposited into the pores react with H_2SO_4, and the specific surface and pore area increase, while average pore diameter decrease. So the samples immersed in H_2SO_4 also lead the

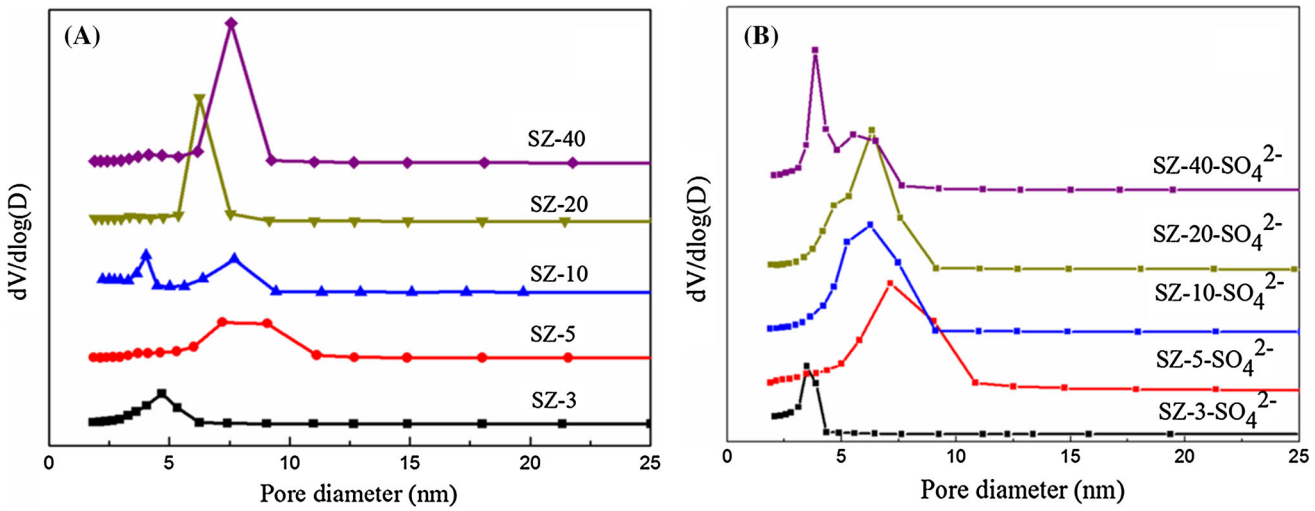

Fig. 4 Pore size distributions calculated by BJH model based on desorption curves of the samples with different Si/Zr calcined at 823 K. **a** Without immersed in H_2SO_4. **b** After immersed in H_2SO_4

Table 1 Physicochemical properties of the caclined samples included co-templates with different Si/Zr calcined at 823 K

Sample	BET surface area (m^2/g)	Micropore area (m^2/g)	Pore volume (cm^3/g)	Average pore size(nm)
SZ-3	412	14.92	0.5	4.84
SZ-3-SO_4^{2-}	606	93.81	0.44	3.36
SZ-5	462	32.84	0.91	7.86
SZ-5-SO_4^{2-}	639	35.61	0.85	6.53
SZ-10	613	40.66	1.1	7.17
SZ-10-SO_4^{2-}	596	38.59	0.92	6.17
SZ-20	765	42.64	1.18	6.14
SZ-20-SO_4^{2-}	664	57.55	0.98	5.89
SZ-40	829	52.59	1.52	7.35
SZ-40-SO_4^{2-}	853	73.69	0.92	4.29

SO_4^{2-} into the structure. When the Zr decreased to 40, the materials did not keep their advantages for the reaction. Thus, the Zr is a significant factor to obtain the micro/mesoporous SiO_2–ZrO_2 materials.

Ammonia adsorption–desorption technique is generally used to determine the strength and amount of acid sites present on the surface of catalyst. Usually, the low temperature desorption peak below 473 K is due to surface hydroxyl groups from weak acid sites. The high temperature desorption peak located at above 573 K is assigned to moderate and strong acid sites [38, 39]. Figure 5 shows the NH_3-TPD profiles for samples calcined at 823 K with different Si/Zr ratio. It can be found that SZ-10-SO_4^{2-} exhibit a relative narrow NH_3 desorption peak starting from 373 to 523 K, which is attributed to the adsorption of the weak acid sites. With the increasing of zirconium content, the peak of weak acid sites widened, illustrating the weak acid sites increased. Notably, SZ-10-SO_4^{2-} has a broad peak from 573 K to 773 K, SZ-5-SO_4^{2-} just has an increased trend on 573 K, however, SZ-3-SO_4^{2-} has no strong acid sites. The reason for this phenomenon may be that with the increasing of zirconium, parts of the channel structure are occupied so that the pore size becomes smaller, and the amount of micropores increased. As we know, microporous materials have a high acidity, thus, the acidity of final samples obtained changed. In another word, the acidity was influenced by the content of zirconium and the amount of micropores. The temperature programmed desorption of ammonia datum are presented in Table S1.

The TEM images of the samples calcined at 823 K show the structure of the samples with different Zr content. The images for SZ-10, SZ-20 and SZ-40 all exhibit very ordered pore structure, whose pores are arranged in a hexagonally ordered array. The pore size is about 5–8 nm

in regular sizes and shapes, as shown in Fig. 6c, d. If making a local enlargement, the cycle-like micropores are vividly observed. The degree of the orderly structure decreases with increasing the content of Zr, which is compatible with the N_2 adsorption–desorption isotherms. As illustrated in the Fig. 6a ordered structures disappeared, moreover, some worm-like pores can be found through the local enlargement and more micropores appeared, illustrating the excess Zr can affect the conformation of the samples. The morphology of the sample SZ-10 calcined at 823 K is shown in the Fig. 6f, which exhibits worm-like shapes. In addition, no large clusters of zirconia nanoparticles are visible at the magnifications used, which indicates that the zirconia is present as either very small nanoparticles or incorporated into the silica framework.

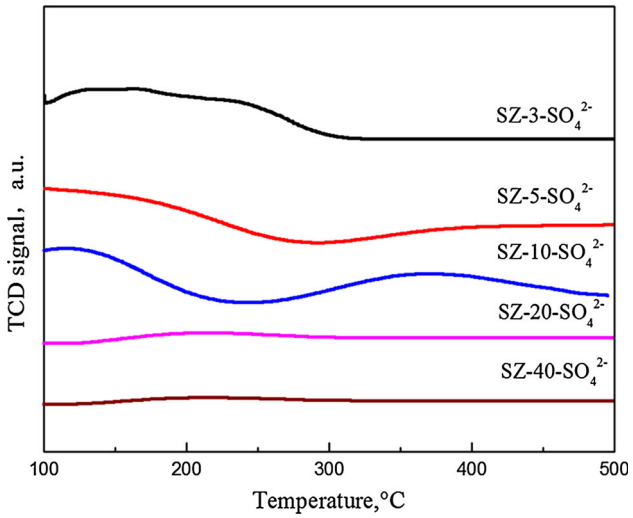

Fig. 5 NH_3-TPD profiles of calcined composite materials with different Si/Zr ratios calcined at 823 K

The catalytic performance of the samples are investigated owing to the samples contain high surface area, narrow size distribution and the addition of zirconium which are favorable for the reaction. The catalytic activity of different solid acid catalysts calcined at 823 K is shown in Table 2. From the table, it is shown that the sample SZ-3-SO_4^{2-}, SZ-5-SO_4^{2-} and SZ-10-SO_4^{2-} all exhibit higher catalytic properties. Among the catalysts, the sample SZ-10-SO_4^{2-} exhibites best catalytic performance. This is probably attributed to the increasing of acid sites with Zr content increased. Combined with the Table 1, it can be seen that SZ-10 has larger specific surface area and bigger pore size than SZ-5 and SZ-3. In addition, SZ-40 and SZ-20 contain a small amount of zirconium, so they display weak force with H_2SO_4 and have a poor catalytic activity. Hence, catalytic activity is not only related to specific surface area and pore size but also associated with the acidity of catalysts. That is to say, the large specific surface area, suitable pore size and high acid intensity are

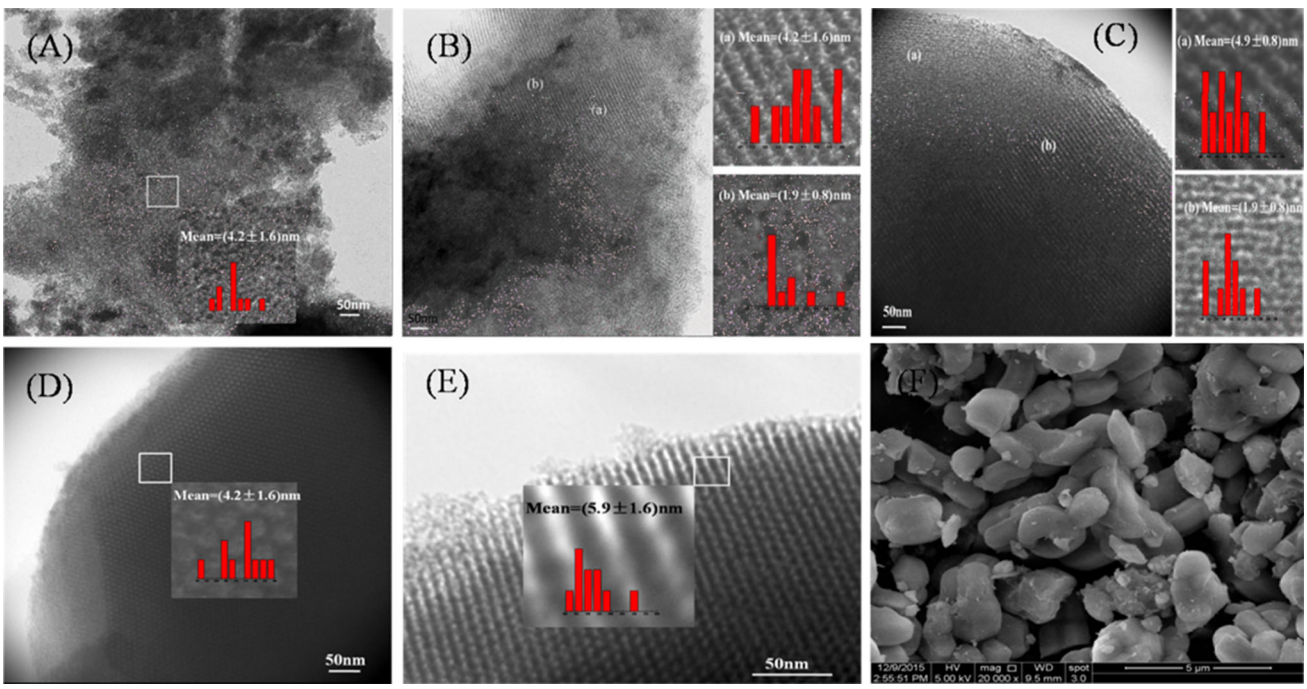

Fig. 6 The TEM image of the samples with different Si/Zr calcined at 823 K. **a** SZ-3, **b** SZ-5, **c** SZ-10, **d** SZ-20, **e** SZ-40, **f** the SEM image of SZ-10. The *insets* in the pictures and the *small pictures* on the right are the local enlargement with the same enlargement scale. *Insets* in each picture were the size distribution histograms

Table 2 Activity of various Si/Zr sulfated catalysts[a] in alkylation of *o*-xylene with styrene

Catalysts	Yield[b] (%)	Selectivity[c] (%)
SZ-3	87.75	90.20
SZ-5	85.37	86.35
SZ-10	94.53	94.80
SZ-20	33.08	37.36
SZ-40	24.23	25.59

[a] Reaction conditions *o*-xylene:styrene = 7.5:1, reaction temperature = 393 K, reaction time = 3 h

[b] Isolated yield based on the amount of styrene

[c] Target product: all products

beneficial to the reaction. Hence, further studies were carried out with SZ-10.

3.2 Effect of calcination temperature

XRD studies were carried out to further illustrate the crystallinity of the obtained SiO_2–ZrO_2 micro/mesoporous materials with Si/Zr = 10 calcined at different temperatures. As shown in Fig. 7, the sample calcined at 823 K has no obvious diffraction peak of zirconium. With the increase of calcination temperature, the samples display broad peaks at $2\theta = 30°$ and 50°, which corresponds to (011) and (112) plane diffraction of the tetragonal phase respectively. The broad and weak peaks indicate the poor crystallinity and small size of tetragonal ZrO_2. XRD peak intensities of tetragonal ZrO_2 increase and the width of the peaks becomes narrower when the samples are treated by calcination process, implying the formation of larger

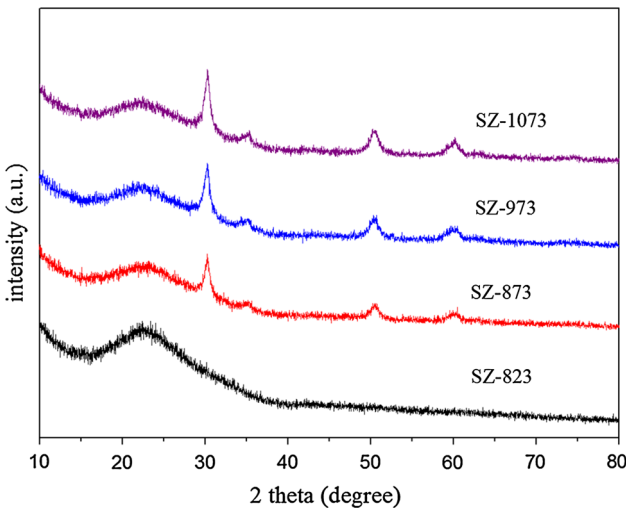

Fig. 7 XRD pattern of the samples Si/Zr = 10 with different calcined temperature

tetragonal crystallites and the enhancement of crystallization. As the calcination temperature increases, the peaks corresponding to tetragonal ZrO_2 are enhanced accordingly. It is reasonable to conclude that the crystallinity of tetragonal ZrO_2 can be controlled by tuning the calcination temperature.

The nitrogen adsorption–desorption isotherms and the pore size distributions for the samples calcined at different temperatures are shown in Fig. 8. As seen from Fig. 8a, the adsorption–desorption isotherms of the synthesized materials show type IV curves with different type hysteresis loops and narrow pore diameter distributions (Fig. 8b). This phenomenon indicates as the zirconium crystal grows up, pore size turns to smaller and smaller, which agrees with the XRD results. Notably, the sample calcined at 1073 K appears two peaks, while the others are only one peak. The reasons for this phenomenon may be collapse of most of the structure channels owing to too high calcination temperature.

Acidic properties of the samples Si/Zr = 10 with different calcination temperatures are investigated by NH_3-TPD analysis, with the TPD profiles presented in Fig. 9 and the TPD of ammonia data are presented in Table S1. Clearly, no obvious desorption peak can be seen in both SZ-823 and SZ-873, indicating that the two catalysts lack strong acid sites and weak acid sites. Also, it can be observed that SZ-973 exhibits one NH_3 desorption peak around 623 K, suggesting that the catalyst has the strong acid sites. However, compared to SZ-973, the desorption peak located at lower temperature (573 K) of SZ-1073 become narrow and which indicates that the strong acid sites of SZ-973 are more than SZ-1073 sample. The reason for this phenomenon may be that with the calcination temperature increasing, the mesochannel of SZ-1073 were destroyed and the micropores increased (Fig. 8b), thus the strong acid sites decreased. Meanwhile, due to the higher calcination temperature, the crystallinity of tetragonal ZrO_2 increased (Fig. 7) and the weak acid sites decreased. The structure of SZ-SO_4^{2-} and acid sites on the SZ-SO_4^{2-} are presented in Schemes 1. From the Schemes 1, the central metal ion acts Lewis sites and the inductive effect of S=O in sulfate complex strongly influenced its acid strength. Due to the O–H bond weakened by the inductive effect of neighboring sulfate groups, Brönsted acid sites were obtained [40].

The structure patterns deriving from the N_2 isotherm are given in Table 3. From the table, it can be seen that with the calcination temperature increasing, BET surface area, micropore surface area and average pore size all decrease gradually. When the temperature increases to 1073 K, the micropore surface area and average pore size decrease to 0.69 $cm^3\ g^{-1}$ and 5.56 nm respectively, which is similar to the sample calcined at 973 K (0.65 $cm^3\ g^{-1}$ and 5.65 nm),

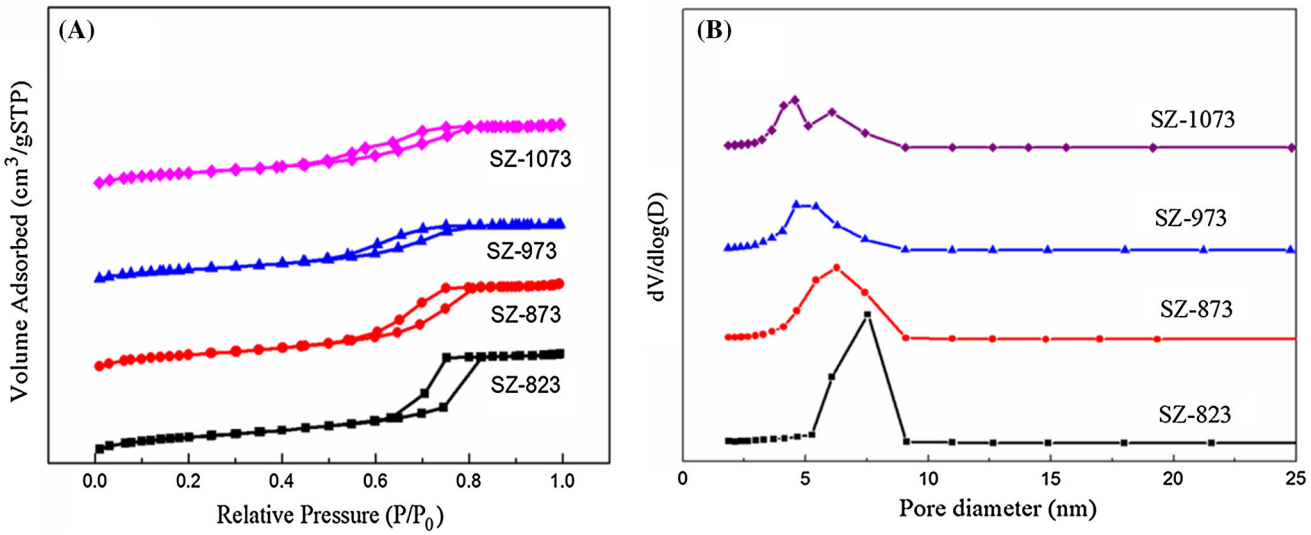

Fig. 8 **a** N_2 adsorption–desorption isotherms, **b** pore size distributions calculated by BJH model based on desorption curves of the samples Si/Zr = 10 calcined at different temperature

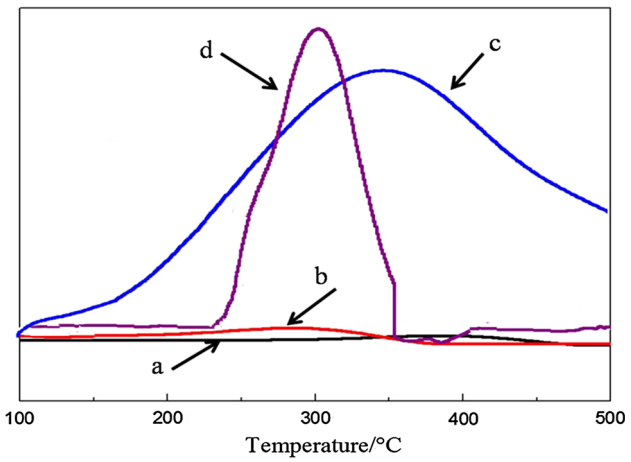

Fig. 9 NH_3-TPD profiles of materials Si/Zr = 10 with different calcined temperature. *a* SZ-823, *b* SZ-873, *c* SZ-973, *d* SZ-1073

certifying when arrive at a certain temperature, ordered pore structure may be damaged but they still keep the micro/mesoporous structure.

To further identify micro/mesoporous material structure properties, TEM of Si/Zr = 10 with different calcination temperatures was performed and the results were shown in Fig. 10. From the figure, all the samples show two kinds of pore channels, micropores and mesopores which are induced by PIL and P123 respectively. In addition, it can be seen that the structure of the materials changed obviously from ordered micro/mesoporous structure to irregular. This is completely the results of the ZrO_2 nanoparticles grow up in the channel structure of micro/mesoporous material. For the sample SZ-1073, a part of walls of mesoporous channels are destroyed in the enlarged picture, which may due to the existence of worm-like micropores. When the temperature decreases to 873 and 823 K, the pores are arranged in an ordered array as observed

Scheme 1 Structure of SZ-SO_4^{2-} and acid sites on the SZ-SO_4^{2-}

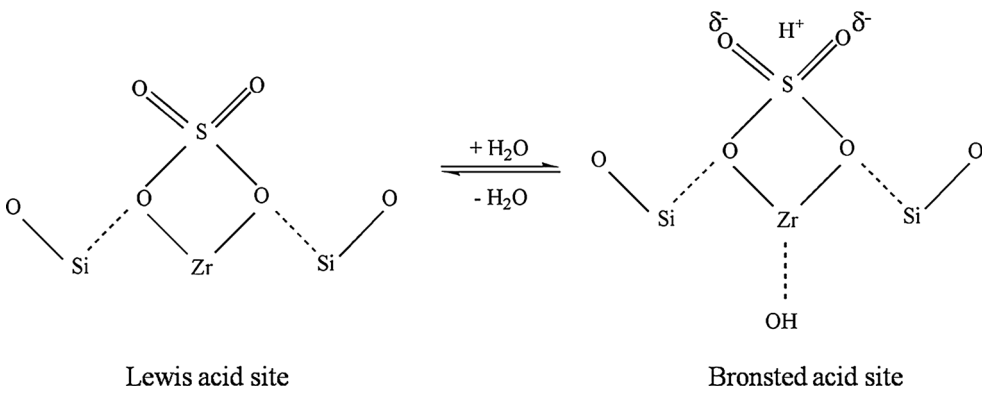

Table 3 Physicochenmical properties of the samples Si/Zr = 10 calcined at different temperature

Sample	BET surface area (m^2g^{-1})	Pore volume ($cm^3\ g^{-1}$)	Average pore size (nm)
SZ-823	613	1.14	7.17
SZ-873	605	0.97	6.37
SZ-973	491	0.65	5.65
SZ-1073	497	0.69	5.56

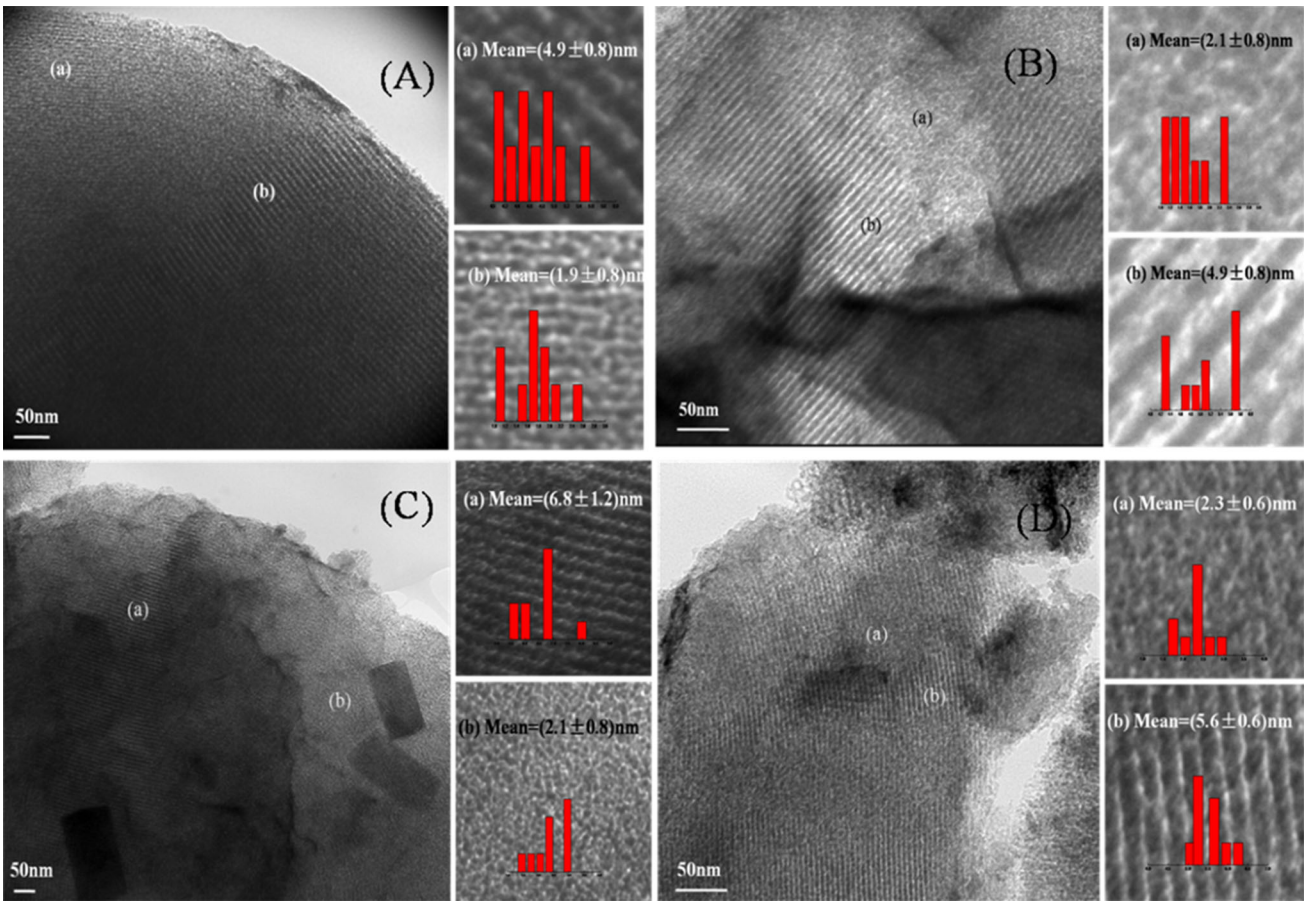

Fig. 10 The TEM image of the samples Si/Zr = 10 calcined at different temperature. **a** SZ-823, **b** SZ-873, **c** SZ-973, **d** SZ-1073. The *pictures* on the right of each image are the local enlargements with the same enlargement scale. *Insets* in each picture were the size distribution histograms

Table 4 Activity of various samples Si/Zr = 10 calcined temperature catalysts in alkylation of *o*-xylene with styrene

Catalysts	Yield (%)	Selectivity (%)
SZ-823	14.6	15.3
SZ-873	23.28	24.04
SZ-973	87.8	88.23
SZ-1073	64.04	66.34

in Fig. 10a, b. And from the images, the samples show a uniform pore size about 6 nm, meanwhile, there still some micropores exist in the samples. Compared with the SZ-1073, SZ-973 has an ordered mesoporous channel, but they have similar BET surface area and average pore size.

The catalytic activity of the samples was evaluated by alkylation reaction and the results are given in Table 4. The detailed reaction scheme is shown in Scheme 2, reaction (1) is the PXE formation reaction whereas reactions (2) and (3) represent the formation of styrene oligomers and more substitutes, respectively. It can be observed that the reaction yield of SZ-823, SZ-873, SZ-973 and SZ-1073 catalysts at 393 K is 14.6, 21.75, 87.8 and 64.04 %, respectively. By comparing with the results of the reaction over various catalysts, the SZ-973 catalyst exhibits the highest catalytic activity among all the catalysts. The reason for this phenomenon is that the enhancement of crystallization of tetragonal ZrO_2 made the strong acid sites for SZ-973 sample be more than that of the other samples with

Scheme 2 Reaction scheme of alkylation of o-xylene with styrene

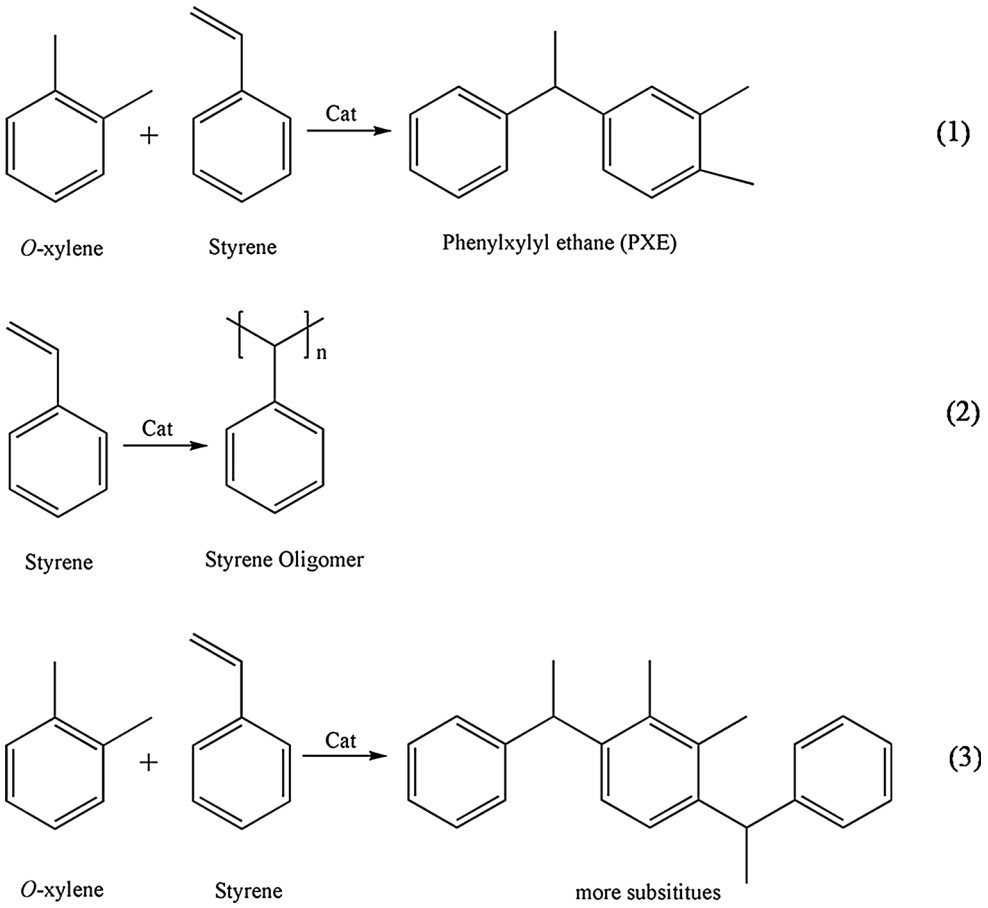

the increase of calcination temperature, which is favorable for the reaction. Moreover, SZ-973 has relatively well-organized mesoporous structure providing places for intermolecular reaction. However, when calcined at 1073 K, because the high temperature has weakened the porous order structure of the samples, the yield and selectivity of the materials decrease.

4 Conclusion

The solid acid catalysts obtained by several zirconium incorporated into micro/mesoporous silica were prepared via a hydrothermal method in the presence of protic ionic liquid as starting materials. Compared with SZ, SZ-SO_4^{2-} still maintained the micro/mesoporous structures. In addition, we also discussed the influence of different calcination temperature on catalytic properties. The introduction of ZrO_2 not only affects the micro/mesoporous structure, but also increases acidity of the material. Furthermore, the materials contain moderate to strong acid sites, the amount of strong acid sites increases with a decrease of Si/Zr ratio. Moreover, the catalytic performances of solid acid catalysts were investigated in the alkylation of *o*-xylene with styrene. Results showed that the micro/mesoporous materials immerged with H_2SO_4 are efficient catalysts for the reaction. The highest yield of PXE (94.53 %) was obtained with the SZ-10-SO_4^{2-} catalyst. This behavior can be related to zirconium doped into the micro/mesoporous framework and generate acid sites, which can increase the interaction between H_2SO_4 and the silica materials and prevent H_2SO_4 leaching from the catalytic materials. It is worth noting that the higher calcination temperature also can make the materials possess good catalytic activities, which is because the enhancement of crystallization of tetragonal ZrO_2 made the strong acid sites increased with the increasing of calcination temperature.

Acknowledgments The authors are grateful to the financial supports of National Natural Science Foundation of China (Grant No. 21376051, 21106017 and 21306023), Natural Science Foundation of Jiangsu Province (Grant No. BK20131288), Fund Project for Transformation of Scientific and Technological Achievements of Jiangsu Province of China (Grant No. BA2014100), The Fundamental Research Funds for the Central Universities (3207046302, 3207045421, 3207046409) and A Project Funded by the Priority Academic Program Development of Jiangsu Higher Education Institutions (Grant No. 1107047002).

References

1. A.B. Dixit, G.D. Yadav, React. Funct. Polym. **31**, 251–263 (1996)
2. J.H. Lunsford, H. Sang, S.M. Campbell, C.H. Liang, R.G. Anthony, Catal. Lett. **27**, 305–314 (1994)
3. X.L. Sheng, Y.M. Zhou, Y.W. Zhang, Y.Z. Duan, Z.W. Zhang, Y.L. Yang, Microporous Mesoporous Mater. **161**, 25–32 (2012)
4. T. Jiang, Q. Zhao, M. Li, H. Yin, J. Hazard. Mater. **159**, 204–209 (2008)
5. F. Chen, H. Ma, B. Wang, J. Hazard. Mater. **147**, 964–970 (2007)
6. J.R. Sohn, S.H. Lee, J.S. Lim, Catal. Today **116**, 143–150 (2006)
7. J. Zhou, Z.L. Hua, W. Wu, Z.C. Liu, Y. Zhu, Y. Chen, J.L. Shi, Dalton Trans. **40**, 12667–12669 (2011)
8. H.L. Chen, J. Ding, Y.M. Wang, New J. Chem. **38**, 308–316 (2014)
9. J. Hu, F. Gao, Y.Z. Shang, C.J. Peng, H.L. Liu, Y. Hu, Microporous Mesoporous Mater. **142**, 268–275 (2011)
10. L.X. Zhang, M. Zhu, L.M. Guo, L. Li, J.L. Shi, Catal. Lett. **1**, 14–18 (2009)
11. J.A. Navio, G. Colon, M. Macias, J.M. Campelo, A.A. Romero, J.M. Marinas, J. Catal. **161**, 605–613 (1996)
12. Y. Zhang, K. Zhu, X. Zhou, W. Yuan, New J. Chem. **38**, 5808–5816 (2014)
13. L.N. Zhao, Y.L. Dong, X.L. Zhan, Y. Cheng, Y.J. Zhu, F.L. Yuan, H.G. Fu, Catal. Lett. **142**, 619–626 (2012)
14. A.T. Shah, B.S. Li, Z.E.A. Abdalla, J. Colloid Interface Sci. **336**, 707–711 (2009)
15. X. Li, B.S. Li, H.H. Mao, A.T. Shah, J. Colloid Interface Sci. **332**, 444–450 (2009)
16. R. Maheswari, V.V. Srinivasan, A. Ramanathan, M.P. Pachamuthu, R. Rajalakshmi, G. Imran, J. Porous Mater. **22**, 705–711 (2015)
17. R. Maheswari, M.P. Pachamuthu, A. Ramanathan, B. Subramaniam, Ind. Eng. Chem. Res. **53**, 18833–18839 (2014)
18. F. Gonella, G. Mazzi, A. Quaranta, P. Soc, Photo. Opt. Ins. **1513**, 425–433 (1991)
19. Sridhar Komarneni, Rajyalakshmi Pidugu, Vinayan C. Menon, J. Porous Mater. **2**, 99–106 (1996)
20. R. Gomez, F. Tzompantzi, T. Lopez, O. Novaro, React. Kinet Catal. L. **53**, 245–251 (1994)
21. K. Kamiya, S. Sakka, J. Mater. Sci. **15**, 2937–2939 (1980)
22. D. Nedumaran, A. Pandurangan, J. Porous Mater. **4**, 897–908 (2012)
23. H. Liu, Y. Su, H.J. Hu, W.R. Cao, Z. Chen, Adv. Powder Technol. **24**, 683–688 (2013)
24. J.D. Mccullough, K.N. Trueblood, Acta. Crystallogr. **12**, 507–511 (1959)
25. A.J. Ward, A.A. Pujari, L. Costanzo, A.F. Masters, T. Maschmeyer, Catal. Today **178**, 187–196 (2011)
26. X. Chen, Z.Q. Sun, L.L. Zheng, Z.M. Chen, Y.F. Wang, N. Fu, K. Zhang, X. Yan, H. Liu, L. Jiang, B. Yang, Adv. Mater. **16**, 1632 (2004)
27. C.H. Christensen, J. Rass-Hansen, C.C. Marsden, E. Taarning, K. Egeblad, ChemSusChem **1**, 283–289 (2008)
28. R. Sheldon, Chem. Commun.**23**, 2399–2407 (2001)
29. X. Feng, Y. Xia, Appl. Surf. Sci. **258**, 2433–2438 (2012)
30. C.C. Ke, J. Li, X.J. Li, Z.G. Shao, B.L. Yi, RSC Adv. **2**, 8953–8956 (2012)
31. S. Zhao, X.L. Sheng, Y.M. Zhou, M. He, X.Q. Fu, Y.W. Zhang, J. Porous Mater. **22**, 1407–1416 (2015)
32. S. Zhao, M. He, Y.M. Zhou, X.L. Sheng, X.Q. Fu, Y.W. Zhang, RSC Adv. **5**, 28124–28132 (2015)
33. M. Zhang, Y. Zhang, X. Sheng, Y. Zhou, S. Zhao, X. Fu, H. Zhang, RSC Adv. **6**, 35076–35085 (2016)
34. K. Zhu, F. Pozgan, L. D'Souza, R.M. Richards, Microporous Mesoporous Mater. **91**, 40–46 (2006)
35. T.L. Merrigan, E.D. Bates, S.C. Dorman, J.H. Davis, Chem. Commun. **23**, 2051–2052 (2000)
36. Y. Zhou, M. Antonietti, Adv. Mater. **15**, 1452–1455 (2003)
37. Y. Zhou, J.H. Schattka, M. Antonietti, Nano Lett. **4**, 477–481 (2004)
38. T.S. Jiang, J.L. Cheng, W.P. Liu, L. Fu, X.P. Zhou, Q. Zhao, H.B. Yin, J. Solid State Chem. **218**, 71–80 (2014)
39. A. Sakthivel, S.K. Badamali, P. Selvam, Microporous Mesoporous Mater. **39**, 457–463 (2000)
40. J.R. Sohn, S.H. Lee, J.S. Lim, Catal. Today **116**, 143–150 (2006)